Remote Sensing of Environment 115 (2011) 3080–3090

Contents lists available at ScienceDirect

Remote Sensing of Environment

journal homepage: www.elsevier.com/locate/rse

Identification and analysis of urban surface temperature patterns in Greater Athens, Greece, using MODIS imagery

Iphigenia Keramitsoglou [a,*], Chris T. Kiranoudis [b], Giulio Ceriola [c], Qihao Weng [d], Umamaheshwaran Rajasekar [d]

[a] Institute for Space Applications and Remote Sensing, National Observatory of Athens, Metaxa & Vassileos Pavlou Str, GR 152 36, Palea Penteli, Athens, Greece
[b] School of Chemical Engineering, National Technical University of Athens, Zografou Campus, GR 157 80, Athens, Greece
[c] Planetek Italia S.r.l., via Massaua, 12-70132 Bari, Italy
[d] Center for Urban and Environmental Change, Department of Earth & Environmental Systems, Indiana State University, Terre Haute, IN 47809, USA

ARTICLE INFO

Article history:
Received 28 December 2010
Received in revised form 6 June 2011
Accepted 15 June 2011
Available online 22 July 2011

Keywords:
Land Surface Temperature
Urban Heat Island
Data mining
Object-based analysis
MODIS

ABSTRACT

Thermal infrared images are being acquired by satellites for more than two decades enabling studies of the human-induced Urban Heat Island (UHI) phenomenon. As a result, the requirement of the scientific community for fast and efficient methods for extracting and analyzing the thermal patterns from a vast volume of acquired data has emerged. The present paper proposes an innovative object-based image analysis procedure to extract thermal patterns for the quantitative analysis of satellite-derived Land Surface Temperature (LST) maps. The spatial and thermal attributes associated with these objects are then calculated and used for the analyses of the intensity, the position and the spatial extent of UHIs. A case study was conducted in the Greater Athens Area, Greece. More than 3000 LST images of the area acquired by MODIS sensor over a decade were analyzed. Three daytime hot-spots were identified and studied (Megara, Elefsina-Aspropyrgos and Mesogeia). They were all found to exhibit similar behavior, gradually increasing their maximum temperature during the summer season and reaching their maxima in mid-July. The hot-spots' thermal intensities compared to a suburban area were of 9–10 °C and were found to be highly correlated to their areal extent. During the night-time, Athens center developed a typical UHI spatially coinciding with the dense urban fabric. The nighttime maximum LST peaked (on average) at the end of July, two weeks later than the daytime surface patterns. The mean spatial extent of UHI in Athens was 55.2 km^2, whilst its mean intensity was 5.6 °C. The proposed automatic extraction process can be customized for other cities and potentially used for comparison of LST patterns and UHI behavior between different cities.

1. Introduction

Knowledge of Land Surface Temperature (LST) and its temporal and spatial variations within a city environment is of prime importance to the study of urban climate and human–environment interactions (Hung et al., 2006; Stathopoulou & Cartalis, 2009; Weng, 2009; Weng & Quattrochi, 2006). Studies on surface Urban Heat Islands (SUHI) and LST distribution within a city have been carried out mostly by using ~1 km spatial resolution satellite sensors, such as AVHRR (Advanced Very High Resolution Radiometer) or MODIS (Moderate Resolution Imaging Spectroradiometer) (Balling & Brazel, 1988; Caselles et al., 1991; Dousset & Gourmelon, 2003; Gallo & Owen, 1998; Gallo et al., 1993a,b; Hung et al., 2006; Kidder & Wu, 1987; Lee, 1993; Rajasekar & Weng, 2009; Roth et al., 1989; Stathopoulou et al., 2004; Streutker, 2002). The LST of urban surfaces correspond closely to the distribution of land use and land cover (LULC) characteristics (Lo et al., 1997; Weng, 2001, 2003; Weng et al., 2004). Moderate and high spatial resolution thermal infrared imagery, such as those from Landsat TM/ETM+, ASTER (Advanced Spaceborne Thermal Emission and Reflection Radiometer), and airborne ATLAS data, have been extensively employed to study intra-urban temperature variations and to relate them to surface cover characteristics (Aniello et al., 1995; Carnahan & Larson, 1990; Kim, 1992; Nichol, 1994, 1996, 1998; Stathopoulou & Cartalis, 2007a; Weng et al., 2006, 2008; Xiao et al., 2008). However, the utilization of high and moderate spatial resolution images in urban climate studies is somewhat restricted because of the limited available data (especially night-time images) and low temporal resolution (Stathopoulou & Cartalis, 2009). To bridge the gap, Pu et al. (2006) assessed data from thermal sensors with different spatial resolutions, including ASTER and MODIS, and concluded that the MODIS thermal sensor can be used for the synoptic overview of an urban area, and that the ASTER sensor can be used for a more accurate/detailed determination of thermal patterns and LST.

* Corresponding author. Tel.: +30 210 810 9167; fax: +30 210 613 8343.
E-mail addresses: ik@noa.gr (I. Keramitsoglou), kyr@chemeng.ntua.gr (C.T. Kiranoudis), ceriola@planetek.it (G. Ceriola), qweng@indstate.edu (Q. Weng), rumahesh45@gmail.com (U. Rajasekar).

0034-4257/$ – see front matter © 2011 Elsevier Inc. All rights reserved.
doi:10.1016/j.rse.2011.06.014

Despite the large number of publications on LST and Urban Heat Islands (UHI) studies using satellite and airborne sensors, Voogt and Oke (2003) criticized that thermal remote sensing of urban areas had been slowly progressed due largely to qualitative description of thermal patterns and simple correlations between LST and LULC types. Furthermore, Xiao et al. (2008) noticed that little research has been done on the statistical relationship between LST and non-biophysical factors. Recent review articles by Weng (2009) and Stathopoulou and Cartalis (2007a), as well as the editorial of the special issue of Remote Sensing of Environment "Thermal remote sensing of urban areas" by Weng and Quattrochi (2006) examined research progresses in this particular field, identified existing problems, and speculated on its future development. A key issue in the application of TIR remote sensing data in urban climate studies is how to use LST measurements at the micro-scale to characterize and quantify surface temperature patterns observed at the meso-scale (Weng, 2009). This observation further implies the need for developing automatic extraction methods and customized software to handle efficiently large volumes of satellite data used for spatial–temporal analysis. Streutker (2002, 2003) used AVHRR data to quantify the UHI of Houston, Texas, as a continuously varying two-dimensional Gaussian surface superimposed on a planer rural background, and derive the UHI parameters of magnitude (i.e., intensity), spatial extent, orientation, and central location. Hung et al. (2006) adopted the Gaussian method proposed by Streutker (2002) to measure the spatial extents and magnitudes of the SUHIs for eight mega-cities in Asia. They used both daytime and night-time MODIS data acquired over the 2001–2003 period to produce surface temperature maps for the eight cities at 1 km spatial resolution, and revealed their diurnal and seasonal patterns. Hung et al. (2006) studied the relationship between heat islands and surface properties as well as the correlation between SUHI magnitude and city population. Rajasekar and Weng (2009) applied a non-parametric model by using fast Fourier transformation (FFT) to MODIS imagery for characterization of the UHI over space, so as to derive UHI magnitude and other parameters. Weng (2009) in his exhaustive review on thermal infrared remote sensing for urban studies pointed out that in spite of these advances, new methods for estimation of UHI parameters from multi-temporal and multi-location thermal infrared imagery are still needed given the increased interest in urban climate community to use remote sensing data.

The main objective of our study is to develop a fully automated extraction method for the analysis of surface temperature patterns from a large number of LST images. Specifically, we intend to obtain a fast procedure to analyze hundreds of LST maps; to identify and extract surface temperature patterns (hot-spots); to characterize the hot-spots (in terms of spatial extent and intensity); and to investigate any correlations between spatial and thermal attributes, based on a case study of the Greater Athens Area in Greece. The methodology developed comprises consequent modules of data pre-processing, feature extraction, database generation, and data analysis. It must be pointed out that Weng (2009) referred to the confusion that exists in published literature between UHIs and 'surface temperature patterns', and commented that the latter is more meaningful; thus, we have adopted the same terminology in the present paper. We have also used the term 'hot-spots' to help the reader visualize the increased LST of the patterns under discussion compared to the cooler suburban/rural areas.

2. Study area and data sets

2.1. Athens Greater Area, Greece

The study area is the Athens Greater Area, the capital and largest city of Greece. According to the recent census paper of Eurostat (http://epp.eurostat.ec.europa.eu/), the Athens Larger Urban Zone (LUZ) is the 8th most populated LUZ in the European Union with a population of about 4,000,000. The area lies at the southeasternmost edge of the Greek mainland (Fig. 1). Athens sprawls across a central basin bound by four mountains and the Saronic Gulf in the southwest. The basin is bisected by a series of small hills. These specific topographic characteristics make Athens an example of a coastal city located in very complex terrain, where sea-breeze and heat-island circulations interact (Dandou et al., 2009) making it especially interesting for UHI and thermal pattern studies. In terms of climate, Athens enjoys a prolonged warm and dry period during the year with July and August being the hottest and driest months. The normal value of the summer (from June to August) daily maximum temperature at Athens is 31.6 °C (with reference to 1961–1990 period; Founda & Giannakopoulos, 2009). In summer-time the city suffers from heat wave events. Particularly in June 2007 a severe heat wave lasted for seven days reaching temperatures as high as 46 °C.

In the daytime the LST patterns of Athens Greater Area yield the presence of two dominant and one weaker hot-spots as shown in Fig. 1. The two dominant hot spots occur at the Municipalities of Megara (denoted by rectangular '1' in the figure) and Elefsina and Aspropyrgos ('2') whilst the weaker one occurs at the area of Mesogeia ('3'). During night-time a typical UHI is developed related clearly to the urban and industrial zone city center ('4'). These will be exhaustively discussed and analyzed in Section 4.

2.2. Data sets

A nine-year time series of MODIS summer images was analyzed. Specifically, 1085 daytime MODIS-Terra LST images and 1956 nighttime MODIS-Terra and Aqua LST images were produced and archived as part of the requirements of Urban Heat Islands and Urban Thermography project (21913/08/I-LG) funded by the European Space Agency. In total more than 3000 raster LST maps of 1 km spatial resolution were tested and processed using the algorithm described in this paper.

The original MODIS data used in the present study were procured at no charge from the Warehouse Inventory Search Tool (WIST web site) repository. Firstly, the MODIS onboard Terra satellite was considered and all the available scenes covering the area of interest were selected. The subset of the daytime scenes with a central viewing angle larger than 45° was identified and removed, due to the well-documented directional dependence of the LST (Lagouarde & Irvine, 2008).

The selected TERRA images consisted of one day- and one night-time scenes, although a number of days (about 2 days every 6) had no available datasets due to the viewing angle constraint. Consequently, MODIS Aqua images were selected so as to ensure that at least one daytime scene is available per day and 1–2 night-time scenes are also available considering that the UHI effect is more evident during the night. At that stage no cloud coverage limitation was set; nevertheless, this was taken into consideration further in the processing chain.

3. Methodology

Initially the MODIS images were processed and the corresponding LST maps were produced. Thermal pattern analysis was implemented through a series of computational procedures involving consequent modules of data pre-processing, feature extraction and data mining. Hot-spots were then analyzed to reveal spatial–temporal trends, as schematically shown in Fig. 2. The complete algorithmic procedure for the thermal pattern analysis was coded in C# .NET, which includes gap filling, filtering, global thresholding, generation of pixel regions and extracting features from regions. The sequence of procedures is described next.

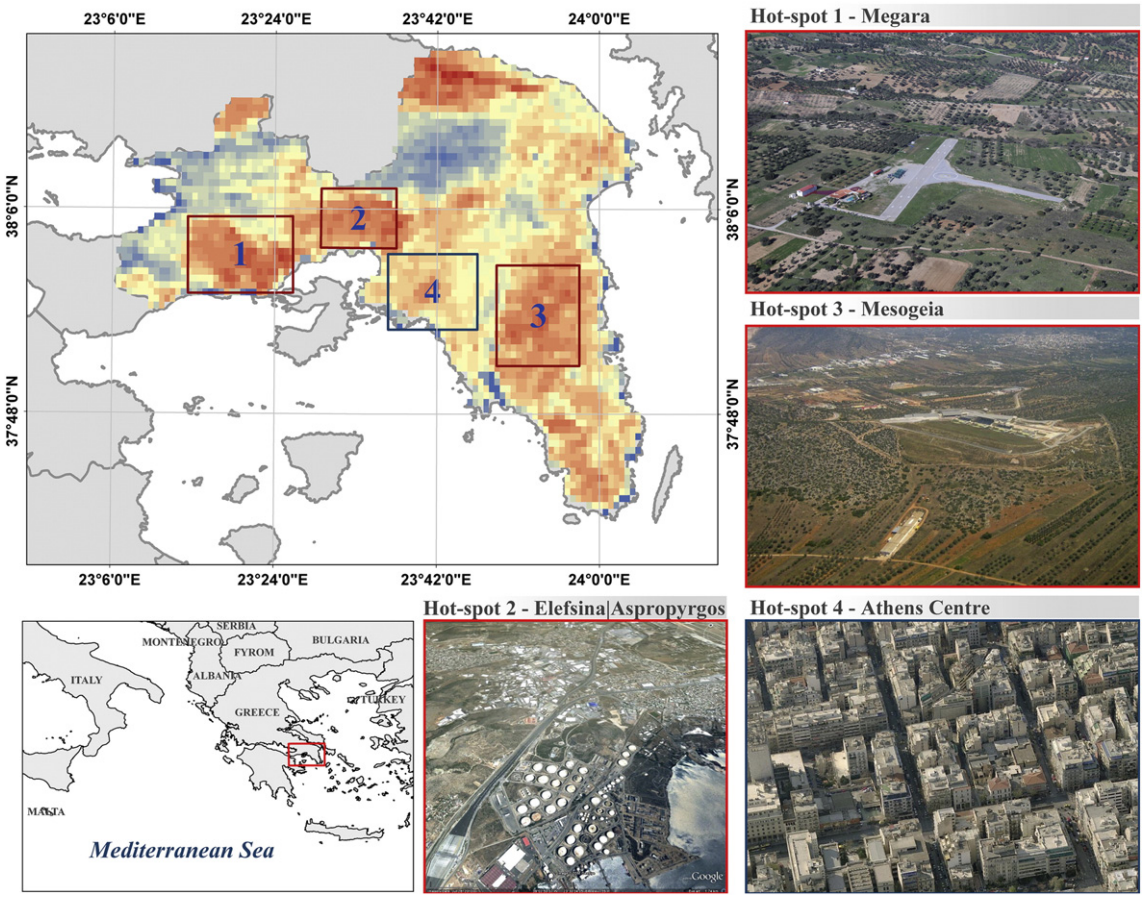

Fig. 1. A typical LST map of Greater Athens Area, Greece, during summer. Numbers 1 to 4 denote the four characteristic surface temperature patterns (hot-spots) of the study area, namely 1: Megara, 2: Elefsina-Aspropyrgos 3: Mesogeia and 4: City Center. A representative subarea of each hot-spot is also provided. (Photo sources: Dounis airfield—I. Saridakis, Google Earth™ mapping service, www.airphotos.gr and Microsoft Bing Maps Platform data, respectively).

3.1. LST computation

The methodology implemented for the calculation of the LST maps is based on the Split Window Technique (SWT) from Jiménez-Muñoz and Sobrino (2008). It has been applied to a number of thermal infrared sensors available today (e.g. ERS ATSR and ATSR2, ENVISAT AATSR, MODIS and NOAA AVHRR) by means of the calibration of some coefficients. The general SWT formula adopted is:

$$T_S = T_i + c_1\left(T_i - T_j\right) + c_2\left(T_i - T_j\right)^2 + c_0 + (c_3 + c_4 PW)(1-\varepsilon) + (c_5 + c_6 PW)\Delta\varepsilon \quad (1)$$

where T_i and T_j are the at-sensor brightness temperatures of the split window bands i and j (in Kelvin), ε is the mean emissivity $\varepsilon = 0.5(\varepsilon_i + \varepsilon_j)$, $\Delta\varepsilon$ is the emissivity difference, $\Delta\varepsilon = \varepsilon_i - \varepsilon_j$, PW is the total atmospheric water vapor content (in g cm^{-2}), and c_0 to c_6 are the SW coefficients specific for each sensor, taken from a predetermined table calculated by Jiménez-Muñoz and Sobrino (2008) with MODTRAN simulations. In the case of the MODIS sensors i and j are bands 31 and 32, respectively. The remaining unknown parameters PW and ε were retrieved using various techniques which have the advantage of needing only the MODIS data itself.

The retrieving of water vapor concentration for daytime images was based on the ratio technique (Sobrino et al., 2003) which uses the MODIS bands in the near infrared spectrum that are most sensitive to PW:

$$PW = 0.192PW_{17} + 0.453PW_{18} + 0.355PW_{19} \quad (2)$$

where

$$\begin{aligned} PW_{17} &= 26.314 - 54.434G_{17} + 28.449G_{17}^2, \quad G_{17} = L_{17}/L_2 \\ PW_{18} &= 5.012 - 23.017G_{18} + 27.884G_{18}^2, \quad G_{18} = L_{18}/L_2 \\ PW_{19} &= 9.446 - 26.887G_{19} + 19.914G_{19}^2, \quad G_{19} = L_{19}/L_2 \end{aligned} \quad (3)$$

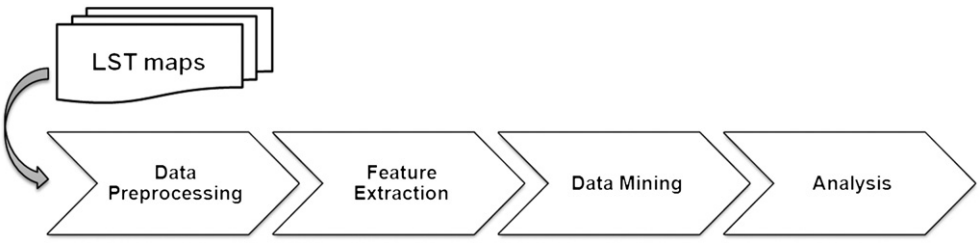

Fig. 2. Schematic representation of consecutive modules for the analysis of surface temperature patterns.

L_i are the radiance measurements acquired by MODIS band i ($i=2$, 17, 18, and 19).

For the night-time images an equation derived from a study of Sobrino et al. (2001) on AVHRR using the Linear Split-Window Relationship (LSWR) was adopted, assuming that bands 4 and 5 of AVHRR are equivalent to bands 31 and 32 of MODIS, respectively:

$$PW = a(T_{31} - T_{32}) + b \tag{4}$$

where T_{31} and T_{32} are the brightness temperatures derived from MODIS bands 31 and 32, respectively. For different emissivities, the slope a and intercept b of Eq. (4) are provided in Sobrino et al. (1999). In particular, for:

- $\varepsilon = 0.96$ ($\Delta\varepsilon = 0.01$), $\alpha = 2.10\ \mathrm{cm^2K^{-1}}$ and $b = 1.93\ \mathrm{gcm^{-2}}$
- $\varepsilon = 0.98$ ($\Delta\varepsilon = 0.00$), $\alpha = 2.21\ \mathrm{cm^2K^{-1}}$ and $b = 1.23\ \mathrm{gcm^{-2}}$
- $\varepsilon = 1.00$ ($\Delta\varepsilon = 0.00$), $\alpha = 2.22\ \mathrm{cm^2K^{-1}}$ and $b = 1.004\ \mathrm{gcm^{-2}}$

All a and b values refer to simulations presented in Sobrino et al. (1999) assuming a negative gradient (between 0 and 5 K) between LST and the temperature of the first boundary layer of the atmosphere.

Finally, the emissivities for bands 31 and 32 were calculated with a simplification of the Normalized Difference Vegetation Index (NDVI) Thresholds Method ($NDVI^{THM}$) introduced by Sobrino et al. (2008). The $NDVI^{THM}$ method uses certain NDVI values (thresholds) to distinguish between soil pixels ($NDVI<NDVI_S$), pixels of full vegetation ($NDVI>NDVI_V$) and mixed pixels ($NDVI_S \le NDVI \le NDVI_V$), assuming the typical threshold values of $NDVI_V = 0.5$ and $NDVI_S = 0.2$. For MODIS

- if $NDVI < 0.2$ then $\varepsilon_{31} = 0.984 - 0.088\rho_1$, $\varepsilon_{32} = 0.982 - 0.028\rho_1$
- if $0.2 \le NDVI \le 0.5$ then $\varepsilon_{31} = 0.974 + 0.015P_v$, $\varepsilon_{32} = 0.968 + 0.021P_v$
- if $NDVI > 0.5$ then $\varepsilon_{31} = \varepsilon_{32} = 0.99$

where ρ_1 is the reflectivity in band 1 and P_V is the proportion of vegetation in a mixed pixel, also referred to as fractional vegetation cover, and is given by

$$P_V = \left(\frac{NDVI - NDVI_S}{NDVI_V - NDVI_S}\right)^2 \tag{5}$$

3.2. LST maps pre-processing

The input data were the MODIS LST products, as described above. The LST maps were in Hierarchical Data Format, commonly abbreviated HDF. The data pre-processing included masking out not valid pixels based on a corresponding flag to assure that only cloud free, not obliquely viewed (>40°) land pixels would be used further in the analysis. Once the valid images and pixels were selected, the problem of missing (flagged) pixels had to be tackled by applying an averaging technique on invalid pixels, where their LST value was actually substituted by the average LST value of their adjacent valid pixels. This procedure, based on a kernel convolution method suggested by Rajasekar and Weng (2009), can be applied in an iterative manner deploying subsequent passes through the invalid pixels of the image. In our case, a single pass was selected as the procedure's critical step since complete restoration would probably produce erroneous patterns within the image. The procedure adopted was necessary in order to facilitate the process of automated information extraction from a large set of images. The resulting image was subsequently filtered using a similar averaging technique as the one presented in the gap filling problem. Filtering was used for smoothing pixel LST so that extreme values were appropriately throttled.

The next step of the pre-processing was the extraction of hot-spot objects through global image thresholding. In the case of global thresholding, the window addressed was the entire image. All pixels whose LST was higher than the suburban LST plus a predefined threshold value (let us say 6 °C) were registered as potential hot pixels. Therefore, the definition of the suburban area, which would serve as the reference area for the analysis, was an important issue. The area selected was the municipality of Thrakomakedones in Attica. The municipality is located at the foot of Parnitha Mt. It is a sparsely built up municipality near a forested area. For each individual image, the procedure evaluated the mean LST for the pixels corresponding to this municipality and hereafter we will refer to this temperature as RLST (Reference Land Surface Temperature). It is stressed that each LST image had its own RLST value. Following the calculation of the reference LST, each pixel LST of the image was compared to RLST.

3.3. Feature extraction

An object-based image analysis procedure was developed to extract hot-spots. According to this procedure, hot pixel image groups were extracted using a global thresholding algorithmic procedure. Separation of hot pixel groups was automatically performed through appropriate segmenting the initial image by partitioning the pixels whose LST value was above a threshold value plus the average LST of reference area pixels. For these pixels, segmentation was performed by determining the k-groups (Pal & Pal, 1993). This type of groups was characterized by a certain proximity property for the pixels of the group, that is to say, each pixel in the group had at least one pixel neighbor that was close to the former by a distance of k pixels in any direction. This distance metric adopted was actually the norm of the digital space processed (image). In this way, depending on the value of k, smaller groups could be merged to bigger ones. In our system, the k pixel distance parameter was set to one (each pixel had at least one neighbor at a distance of one pixel). An algorithm of linear computational complexity was used to separate groups obtained. According to this algorithm each pixel was checked for its neighbors, which in turn were checked for theirs in a recursive way. The grouped pixels were then treated as different regions (objects). Following that, several features related to these objects, which represent the city hot-spots were extracted.

3.4. Data mining

The hot-spots represented as objects underwent a series of procedures to extract the necessary information for the area. As a first step a procedure counted the number of pixels that belonged to each object. If the object area was smaller than 10 km^2 (i.e., number of pixels was less than 10), then the object was not further studied. Only the objects whose weighted centroid belonged to a predefined area of interest were taken into consideration. Four areas of interest were defined, already mentioned in Section 2.1. The results of the above mentioned procedure are illustrated in Fig. 3.

Once the objects of interest were extracted a number of parameters per object were calculated and appropriately stored in a database. These parameters included the satellite sensor as well as temporal, spatial (weighted centroid location, extent in km^2) and thermal information (e.g. minimum, maximum LST). In total, 1237 daytime hot-spots were identified with a 6 °C threshold value and 358 night-time hot-spots with a 4 °C threshold.

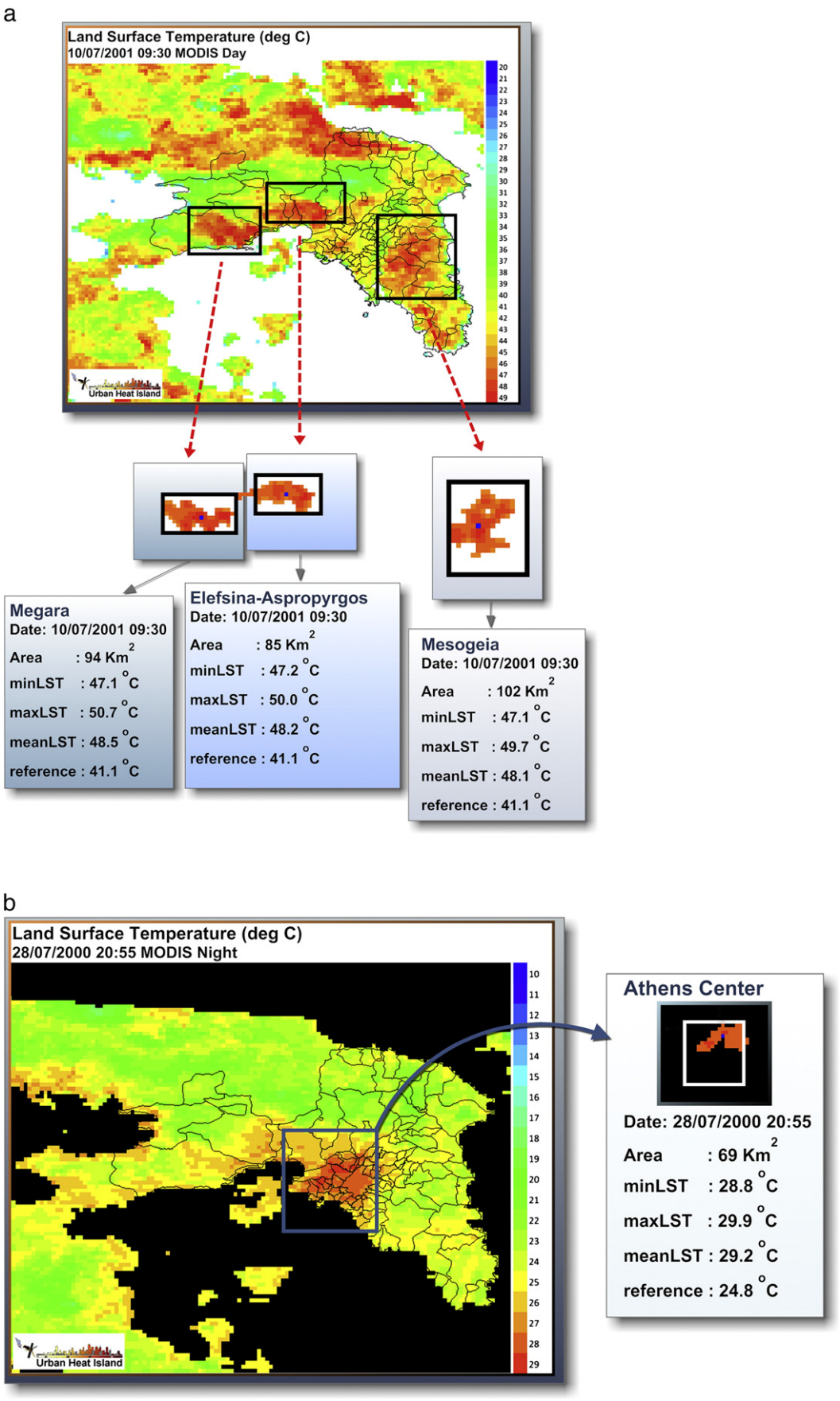

Fig. 3. Schematic representation of the data mining concept. The areas warmer than a reference LST are identified, extracted and subsequently treated as objects. (a) Typical daytime LST map with three hot-spots. The hot-spots are extracted and the relevant spatial and thermal characteristics of the objects are calculated and stored in a database, and (b) Typical night-time LST map representing the UHI of Athens city.

Table 1
Day- and night-time hot-spots of the Athens Greater Area.

Hot-spot	Hot-spot characterization	Municipalities	Corine land cover class	Corine land cover code
1	Dominant, Daytime	Megara	Agricultural land	2.2.3, 2.4.2, 2.3.1
2	Dominant, Daytime	South part of Aspropyrgos and Elefsina	Industrial zone discontinuous urban fabric, airport and agricultural land	1.2.1, 1.1.2, 1.2.4, 2.4.2
3	Weaker, Daytime	At and around Koropion, Paiania, Spata-Loutsas (Mesogeia)	Agricultural land, Airport	2.4.2, 2.2.1, 1.2.4
4	Dominant, Night-time	City of Athens (Athinai), Ilion, Ag. Anargyroi, Nea Halkidona, Peristerion, Egaleo, Kamatero, Nikaia, Keratsinion, Tavros, Ag. Ioanni Renti, Peiraiefs, Moshaton, Kallithea, N. Smyrni, Drapetsona	Urban areas (mainly continuous urban fabric)	Mainly 1.1.1

4. Results

4.1. General thermal pattern in the Greater Athens

Four areas of interest can be defined in the majority of the LST maps for the Athens Greater Area. In particular there are three daytime hot-spots (Hot-spot No. 1, 2, 3; Fig. 1 and Table 1) and one night-time (Hot-spot 4; Fig. 1 and Table 1). On the daytime images (most of which were acquired before 12:00 Local time), surface temperature spatial patterns revealed that the center of Athens did not exhibit the highest LST; this is referred to as urban heat sink or negative heat island. It can be simply considered as a brief stage in the development of the UHI that occurs during the morning and midday period due to differences in the urban–rural warming rates (Oke, 1987). This behavior is well known for Athens, as already reported in Stathopoulou and Cartalis (2007b). Therefore, in the daytime the LST patterns of Athens Greater Area yielded the presence of two dominant and one weaker hot-spots, as presented in Fig. 1 and described in Table 1.

The typical daytime pattern in 3D can be also observed in Fig. 4(a). In this figure the LST images were plotted in a wire frame model to appreciate visually the thermal variations as 'height' (z-axis) and color. Visual analysis of the hot-spots (especially the two dominant ones, hot-spots Nos. 1 and 2; Table 1) showed that there was a LST discrepancy of at least 4–6 °C from the suburban areas. They appeared in almost every morning image of June–August; the phenomenon was weaker in May and September. These hot-spots were clearly identifiable by photo-interpretation of satellite images on all spatial resolutions (from Landsat TM to MSG-Seviri, not shown here). It should be noted that the time of MODIS acquisitions allowed studying of the phenomenon at certain time (around 09:00 UTC; midday 12:00 local summer time). Another interesting feature of Fig. 4(a) is the presence of cooler pixels along the coastline, which may be partially caused by sea breeze. In general, the thermal environment of Athens during daytime depends on the combined influence of the area topography and surface cover characteristics. The open plain of Mesogeia (Hot-spot No. 3, Table 1 and Fig. 1) is mainly covered with sparse low vegetation (particularly olive trees and vineyards) and bare soil (Athens International Airport "El. Venizelos" is also located at this area) whilst Aspropyrgos and Elefsina (Hot-spot No. 2 of Fig. 1) are mainly industrial zones. These plains become warm faster than densely built-up urban areas which are extensively covered by materials of high thermal inertia such as concrete and asphalt. The influence of topography is also evident on the thermal pattern of the study area, as higher altitudes exhibit lower LST.

During the night-time, the thermal pattern of Athens was inverted as higher surface temperatures were related with the residential urban zones rather than the different urban use zones and rural areas. There was one dominant hot-spot affecting a number of central municipalities, as described in Table 1. A 3D representation of a typical night-time LST image is shown in Fig. 4(b). At that time of day, cooling or warming of a surface is determined by its thermal characteristics. Thus, during night hours, the continuous urban fabric is a few degrees warmer than rural areas, due to the lower thermal inertia of the soil compared to concrete. In contrast, the morning hot-spots of the city have faded out in the night and appear to be cooler than the continuous urban fabric owning to the fact that in industrial and agricultural areas usually extended open spaces of bare soil cover most of the area. The presence of a heat wave increases LST and makes less definable the hot-spots.

4.2. Time series of maximum LST

The high volume of data allowed the extraction of statistics and the investigation of possible correlations and trends. In this paper we present the results of the analysis including the behavior of the maximum LST of the different hot-spots over time, the frequency of occurrence of the thermal intensity (discrepancy between hot-spot maximum and RLST), and the correlation between the thermal intensity and the size of the hot-spots.

The maximum LST of the hot-spots (hereafter referred to as maxLST) was analyzed by plotting the maxLST acquired between 08:55 and 10:00 UTC against date (1st May to 30th September) for every year separately and fitting a quadratic polynomial to the data. The reason behind the selection of a certain time window was to eliminate the diurnal variation signal from the analysis. In any case this specific window was the one with most of the daytime MODIS acquisitions ensuring minimum loss of data. The results per year and hot spot are presented in Table 2, whilst for all years are shown in Fig. 5 (day = 0 is the 1st May and day = 152 is the 30th September; the year was irrelevant). The plot clearly shows a consistent seasonal variation with increasing maxLST from the beginning until approximately middle of the season and then the gradual decrease of temperature until the end of the season (end of September). Fig. 5(a) shows the described seasonal trend of Megara Hot-spot (No. 1) with a maximum of 48.6 °C on July 14, after when the maxLST starts decreasing. The same behavior was observed at Elefsina-Aspropyrgos hot-spot (No. 2); in this case the maximum was observed on July 16 and was of the same value. The third slightly weaker hot-spot of Mesogeia (No. 3) was consistently cooler (between 1 and 3 °C; Table 2) compared to the other two dominant hot-spots. As a result the maximum of the overall seasonal trend (Fig. 5(a)) was 2 °C cooler and was observed on July 15.

For the night-time images, a 4 °C threshold was selected for the city center, as it was more realistic and increased the number of objects and subsequently statistical samples. The maxLST for the city center (Fig. 5(b)) follows a similar seasonal pattern. As expected the maxLST was considerably lower than the morning hot-spots. The quadratic line fitted to all the available maxLST night-time data versus day of the season peaked on July 29, two weeks later than the daytime surface patterns. The same behavior was observed for all years (Table 2). By definition, this was the UHI pattern of Athens city.

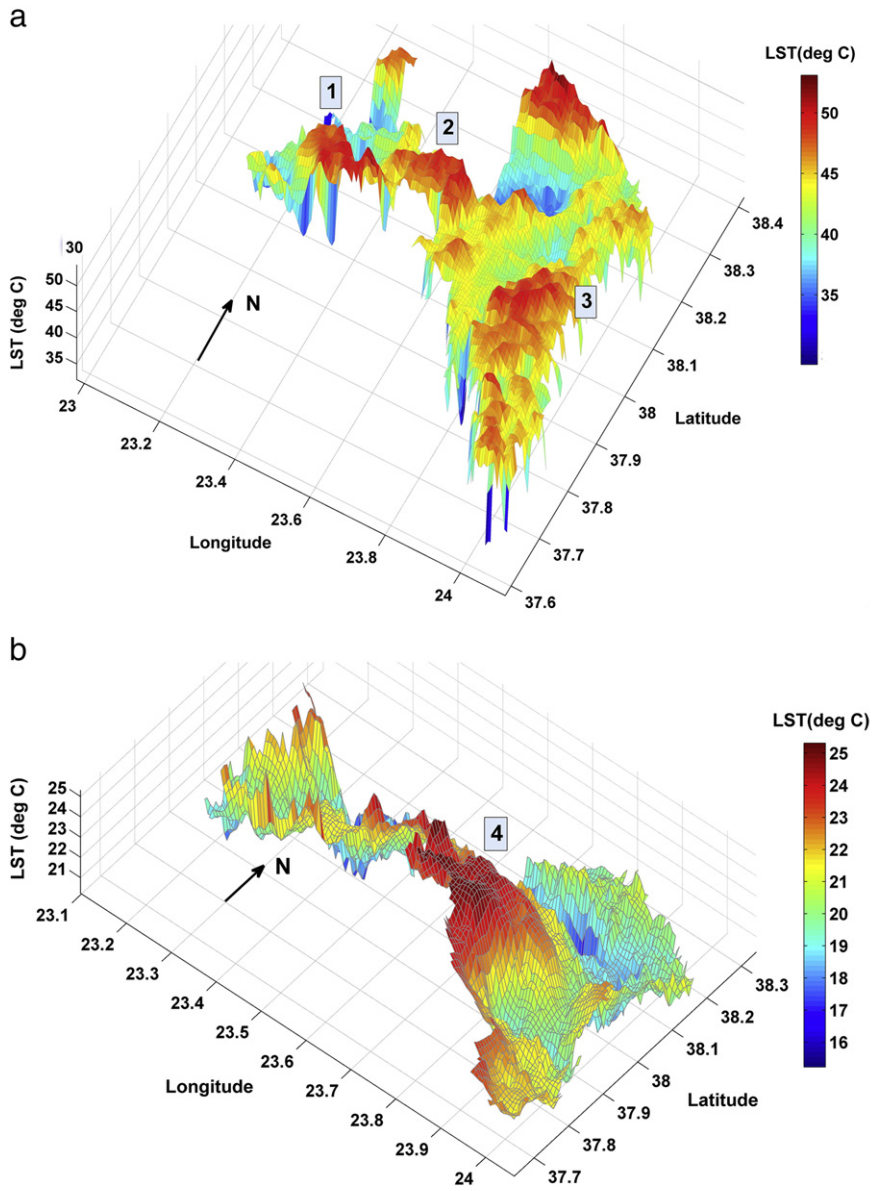

Fig. 4. Typical 3D LST patterns in Athens Greater area using MODIS. (a) Daytime hot-spots 1, 2 and 3. For a fly though a typical daytime LST 3D distribution of Athens Greater Area please visit: http://195.251.203.191/video/daytime.html; (b) Night-time hot-spot 4. A fly though a typical night-can be seen at http://195.251.203.191/video/nighttime.html.

4.3. Hot-spots intensity and extent

By thermal intensity we refer to the discrepancy between the maxLST of a hot-spot and the RLST. In other words, thermal intensity shows the LST difference between the hot-spot and the suburban area. As before, the three daytime hot-spots and the one night-time hot-spot of the urban center were studied. Fig. 6 shows the distribution of the Intensity occurrences per hot-spot by means of histograms. A Gaussian curve was fitted on the original data, for better statistical description of the results. The daytime results for Megara are presented in Fig. 6(a) and for Elefsina-Aspropyrgos in Fig. 6(b). The Intensity occurrences were similar for both areas and both distributions peaked at 10 °C. The corresponding histogram for Mesogeia hot-spot is shown in Fig. 6(c). The Gaussian curve in this case peaked at 9 °C. Fig. 6(d) gives the distribution for the night-time measurements at the City Center, which—by definition—was the UHI magnitude. The fitted curve peaked at 5.7 °C at night-time, decreasing faster than the corresponding daytime curves.

Whilst the intensity was the difference between maxLST and RLST, tDiff was defined as the difference between maximum and minimum LST within the same surface temperature pattern, thus giving a measure of the thermal differences inside an affected area. The mean, the maximum and the absolute (standard) deviation (ADEV) of the

Table 2
Fitted maximum LST of the four hot-spots of Athens Greater Area per year with the corresponding date when it occurred.

Year	Hot-spot							
	1 (Daytime)		2 (Daytime)		3 (Daytime)		4 (Night-time)	
	Date	Max LST	Date	Max LST	Date	Max LST	Date	Max LST
2000	7-Jul	50.2	9-Jul	50.3	10-Jul	47.9	19-Jul	26.4
2001	13-Jul	49.5	15-Jul	49.0	12-Jul	46.3	1-Aug	27.8
2002	11-Jul	47.9	16-Jul	49.1	16-Jul	46.8	30-Jul	26.1
2003	17-Jul	48.0	18-Jul	48.2	19-Jul	45.5	29-Jul	25.8
2004	16-Jul	48.7	18-Jul	49.4	15-Jul	47.0	2-Aug	26.5
2005	17-Jul	48.3	16-Jul	48.0	18-Jul	45.9	29-Jul	25.9
2006	13-Jul	46.6	12-Jul	47.4	12-Jul	45.3	24-Jul	26.1
2007	12-Jul	49.2	14-Jul	48.4	15-Jul	46.9	1-Aug	27.4
2008	12-Jul	50.4	17-Jul	49.1	10-Jul	47.4	27-Jul	26.2

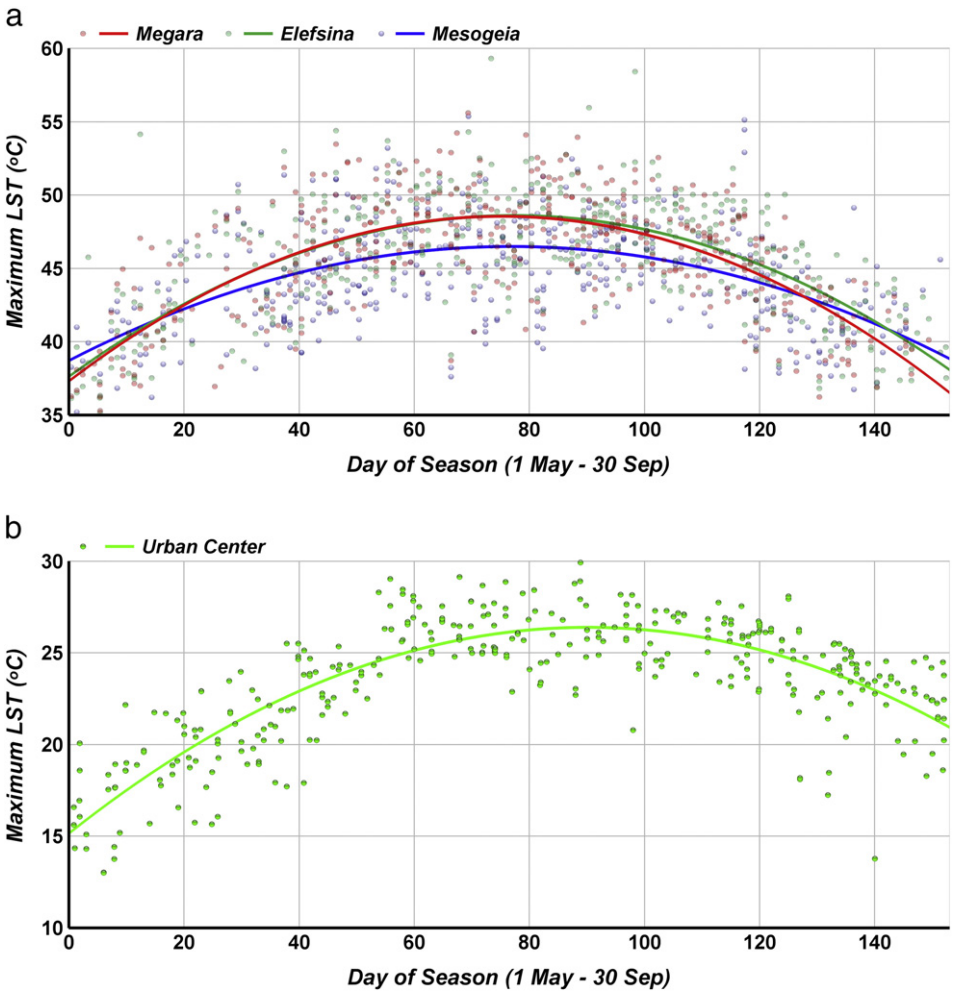

Fig. 5. Maximum LST acquired at (a) the three daytime hot-spots between 08:55 and 10:00 UTC during the summer months (May–September) from 2000 to 2009 as a function of day of season, and (b) Athens City Center hot-spot (No. 4) at night-time for the same period.

hot-spots surface extent, intensity and tDiff were calculated. Table 3 presents the results.

In terms of the surface extent the weaker morning hot-spot of Mesogeia is the largest, the second being the dominant hot-spot of Megara and then of Elefsina, with an average surface of 112.0, 95.2 and 83.5 km^2, respectively. The dominant hot-spot of Elefsina, however, is the least variable one (the ratio ADEV/MEAN of the fitted values is 0.33 compared to 0.61 for the extended and quite variable hot-spot of Mesogeia). In spite of differences in surface extent, all three morning hot-spots are consistent in mean thermal intensity, which varied between 9 and 10 °C with similar statistical spread (ADEV) of the values of less than 1.2 °C. It is interesting to note that the maximum recorded thermal intensity is above 17 °C for all three morning hot-spots and even reached 20.6 °C in Elefsina at 09:40 UTC of 2007-05-13. The mean thermal difference (tDiff) within the morning hot-spots ranges from 3 to 4 °C, although a maximum difference of 14.6 °C inside the hot-spot was recorded in Elefsina on the same satellite acquisition. The standard deviation (ADEV) is between 1.0 and 1.2 °C.

The investigation of the night hot-spot behavior reveals the characteristics of the UHI phenomenon of the center of Athens. The mean surface extent of UHI pattern is 55.2 km^2 using the original values and 3.6 km^2 larger using the gaussian fitted values. The reader is reminded that the night-time patterns are extracted using a 4 °C threshold difference between the hot-spot and the reference suburban area. When increasing the threshold the spatial extent is smaller; for instance for 6 °C threshold the mean is 45.8 km^2. The mean UHI intensity is of 5.6 °C, also shown in Fig. 6(d). A maximum intensity of 12.3 °C was recorded on 2004-09-11 at 20:30 UTC. The mean thermal difference within the UHI pattern (tDiff) is lower than the morning patterns and is equal to 1.6 °C. However, tDiff reached 8.3 °C on the same image.

In the previous paragraphs we have discussed the statistics of the extent of the hot-spots, an interesting parameter as it reveals the area affected by the higher temperatures. Streutker (2002) investigated whether the spatial extent of the heat island was related to the thermal intensity (referred to as UHI magnitude) and to the surrounding rural temperature. This was found not to be the case in his research, as none of these temperature measurements showed significant correlation to the spatial extent. When we investigated similar correlations of the daytime hot-spots of Greater Athens Area, we found that their hot-spot extent was not correlated directly with a thermal feature such as the maxLST or minLST. Nevertheless, our analysis showed that the spatial extent of a hot-spot is highly correlated with its intensity. This is true for all three morning hot-spots whose correlation coefficient is above 0.75, yet not true for the UHI night-time city center phenomenon. In particular, the correlation coefficients for the hot-spots of Megara and Elefsina-Aspropyrgos are 0.79, whilst for Mesogeia is 0.76 (Fig. 7). This correlation is reported for the first time for Greater Athens, since published works has been mostly focused at the city of Athens and its

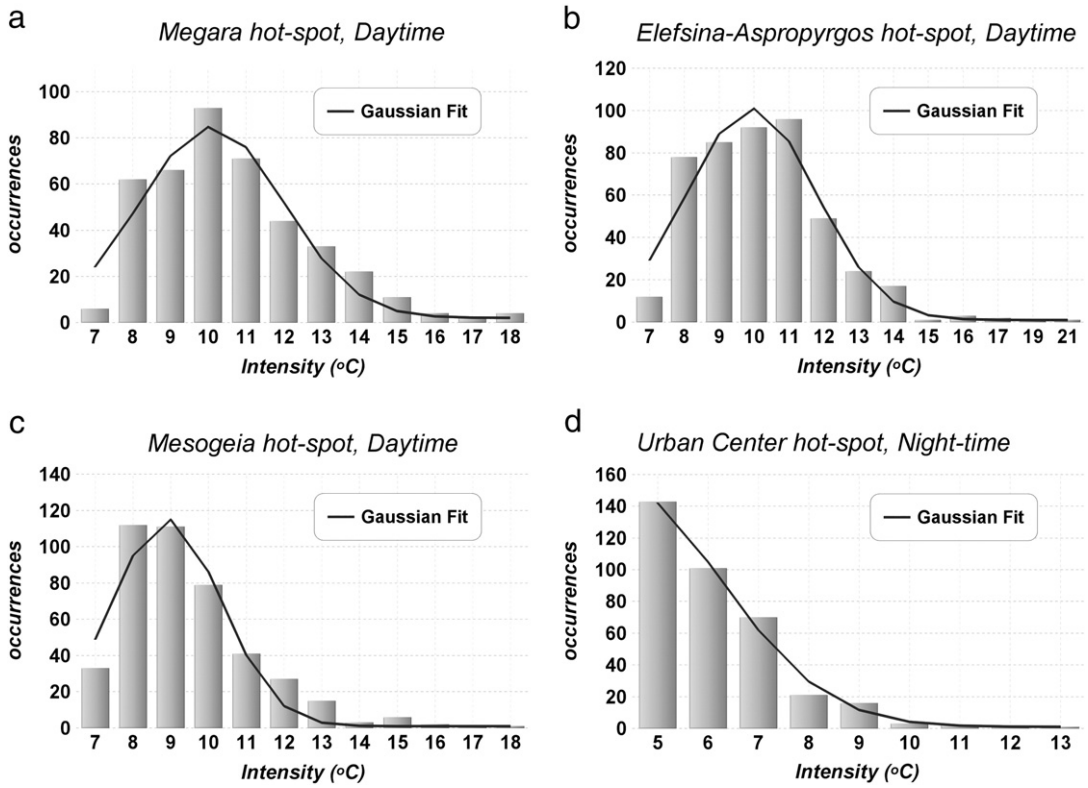

Fig. 6. Histogram representing the occurrences of certain thermal intensities (maxLST-RLST) (a) at Megara dominant hot-spot during daytime, (b) at Elefsina-Aspropyrgos dominant hot-spot during daytime, (c) at Mesogeia weaker hot-spot during daytime, and (d) at Athens City Center during night-time. The latter is the UHI intensity.

immediate vicinity (e.g. Livada et al., 2002; Santamouris et al., 2007; Stathopoulou & Cartalis, 2007a).

In order to explain the observed correlation, one has to consider that LSTs estimated by satellite sensors are the spatial patterns of upwelling thermal radiance received by the remote sensors. A hot-spot is thus the aggregated result of warmer pixels. In general LSTs are higher and more variable than concurrent air temperatures due to the complexity of the surface types in urban environments and variations in urban topography (e.g. Nichol, 1996; Streutker, 2002) and they are more easily related to surface conditions themselves (Imhoff et al., 2010; Nichol & Wong, 2005; Owen et al., 1998; Voogt & Oke, 2003).

Table 3
Statistics related to the characteristics of the three day- and one night-time hot-spots of Athens Greater Area as calculated from MODIS data acquired during the summer months (May–September) of years 2000–2009. Fitted values refer to a quadratic polynomial.

Hot-spot	Statistical parameter	Surface extent (km^2)		Intensity (°C)		tDiff (°C)	
		Data	Fitted	Data	Fitted	Data	Fitted
1 (Daytime)	MEAN	95.2	97.4	10.1	10.2	4.1	4.2
	MAX	561.0	330.5	17.9	14.6	11.8	8.5
	ADEV	47.3	36.2	1.6	1.2	1.6	1.2
2 (Daytime)	MEAN	83.5	86.9	9.8	9.8	3.7	3.8
	MAX	362.0	251.7	20.6	15.6	14.6	9.6
	ADEV	40.8	29.1	1.5	1.0	1.5	1.0
3 (Daytime)	MEAN	112.0	129.0	9.0	9.1	3.0	3.1
	MAX	667.0	474.2	17.3	12.7	11.3	6.7
	ADEV	96.9	79.1	1.4	1.0	1.4	1.0
4 (Night-time)	MEAN	55.2	58.8	5.6	5.7	1.6	1.6
	MAX	315.0	188.0	12.3	9.1	8.3	5.1
	ADEV	45.6	33.4	1.0	0.8	1.0	0.7

The observed daytime correlations presented here are strongly related to the differential heating rate (Oke, 1982; Voogt & Oke, 2003) between open spaces such as bare soil and agricultural land (like in Megara and Mesogeia hot-spots) compared to sparsely built-up vegetated areas as our reference area. Land covered by vegetation has a slower heating rate than bare soil or agricultural land and reaches lower LST. In this work we have defined the thermal intensity as the discrepancy between hot-spot maximum and RLST, and the spatial extent of a hot spot as the area covered by the aggregated cluster of pixels whose LST is higher than the RLST plus a predefined threshold value. Let us now assume solar heating which will result in LST rise. The rise will be higher in the area of the hot-spot than the reference area due to differential heating rate. This in turn will result in a two-fold effect: the thermal intensity will increase and the cluster of warm pixels that will be extracted as thermal pattern will be larger. It is worth noting that a hot-spot would potentially increase in size until a topographic feature, a densely vegetated area or a large water body imposes an abrupt change in the LST distribution (Oke, 1982).

5. Conclusions

This paper introduced an object-based image analysis procedure to extract hot-spots from a large volume of satellite thermal infrared image dataset. A series of attributes was calculated for each hot-spot pattern, i.e., the aeria extent and thermal features, allowing the study of the spatial behavior of thermal patterns with time (over a decade or/and within the summer season). The proposed approach further allowed the investigation of correlations between the attributes. The methodology was applied to more than 3000 MODIS images acquired from May until September from years 2000 to 2009 for the Greater Athens Area in Greece.

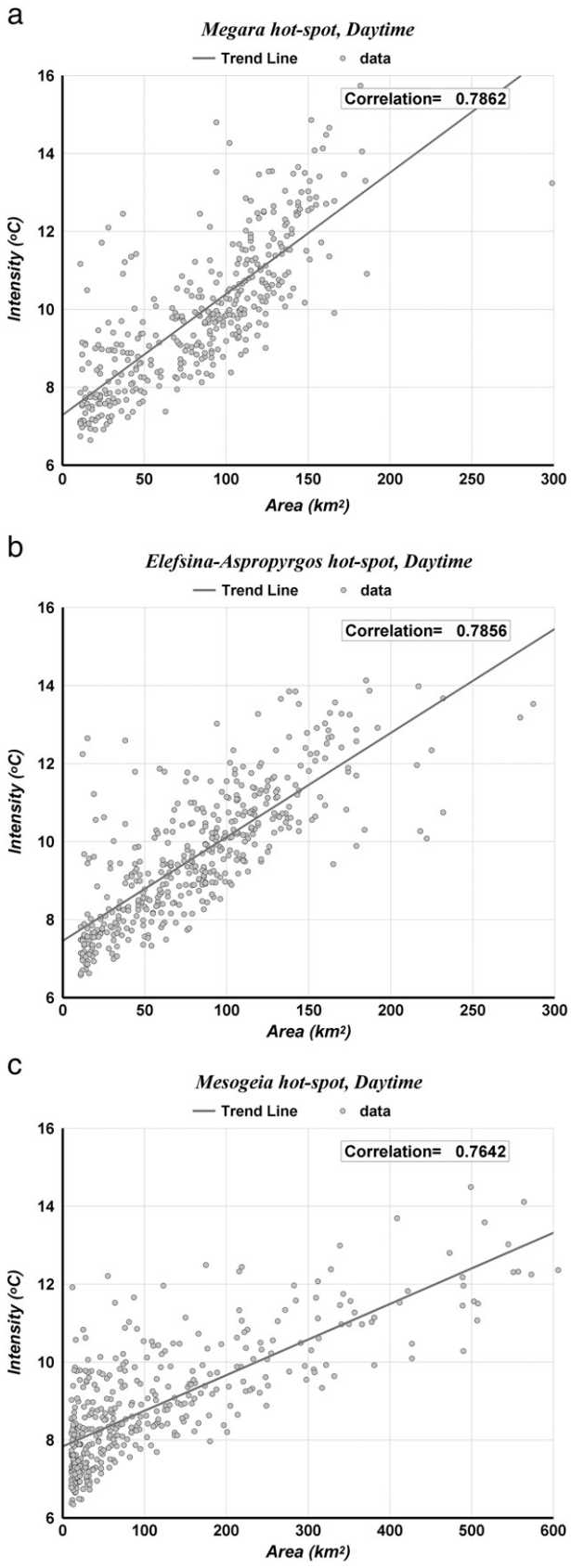

Fig. 7. Correlation between the thermal intensity and the surface extent of the daytime hot-spot of (a) Megara, (b) Elefsina-Aspropyrgos and (c) Mesogeia.

The results show that in MODIS daytime acquisitions three areas consistently appeared warmer than the city center. These areas are Megara, Elefsina-Aspropyrgos and Mesogeia which were mainly covered by sparse low vegetation and bare soil and exhibited faster heating rate than urban areas (negative heat island). On the other hand, the city center of Athens was characterized by a strong UHI phenomenon that was observed later in the day and mostly at night-time. The daytime hot-spots exhibited similar behavior, gradually increasing their temperature during the summer season, reaching their maxima in mid-July. Their thermal intensities were of 9–10 °C. The areal extent was found to be highly correlated to the thermal intensity. During night-time, Athens center developed a typical UHI spatially coinciding with the dense urban fabric. The maximum LST peaked (on average) at the end of July, showing a two-week time lag compared to the daytime surface patterns.

The main innovation of this research is that the thermal hot-spots were extracted and treated as objects. This allowed for the calculation of several features related to the hot spots (e.g., the area extent, the maximum, mean and minimum LST) from the original LST maps. Other recent studies (Rajasekar & Weng, 2009; Streutker, 2003) had dealt with modeled approximations (e.g. fast Fourier transformation; FFT) of the temperature patterns. For instance, Streutker (2003) approximated the area extent of the UHIs by calculating the longitudinal and latitudinal extent assuming an ellipsoid footprint. Additionally, our method was used to extract the attributes and to present them as a series of functions rather than a series of images, as suggested by Rajasekar and Weng (2009). The thermal features retained their original values circumventing modeling and smoothing out the maximum values of the original data. The proposed methodology can be considered appropriate for both coastal cities, where the discontinuity of sea-land interface would cause complications in the modeling approach, as well as inland cities. The methodology can be customized to cover other geographical areas. Nevertheless, sufficient knowledge of a city is required to efficiently define the areas of interest as well as the reference rural/suburban area. Information on the city's land cover and topography is also important for the interpretation of the patterns. However, once the area of interest is set, the algorithm processes thousands of LST images in a few seconds without any manual interference. As comparison of thermal patterns across different cities is currently hampered by the lack of an appropriate methodology to extract the patterns and characterize them, future research should examine the application of the method to different cities and comparison of their UHIs behavior.

Acknowledgments

Special thanks go to Ms. Maria Michelaraki from the Hellenic National Meteorological Service for her contribution regarding the causes of the thermal patterns of Athens. The authors are also thankful to Mr. Themistocles Herekakis (NOA/ISARS) for producing the plots. The MODIS data used for this paper were procured and pre-processed within the framework of Urban Heat Islands and Urban Thermography project (www.urbanheatisland.info, 21913/08/I-LG; European Space Agency). The authors wish to thank the anonymous reviewers for their constructive comments that improved substantially the manuscript.

References

Aniello, C., Morgan, K., Busbey, A., & Newland, L. (1995). Mapping micro Urban Heat Islands using Landsat TM and a GIS. *Comparative Geoscience*, *21*, 965–969.

Balling, R. C., & Brazel, S. W. (1988). High-resolution surface-temperature patterns in a complex urban terrain. *Photogrammetric Engineering & Remote Sensing*, *54*, 1289–1293.

Carnahan, W. H., & Larson, R. C. (1990). An analysis of an urban heat sink. *Remote Sensing of Environment*, *33*, 65–71.

Caselles, V., Lopez Garcia, M. J., Melia, J., & Perez Cueva, A. J. (1991). Analysis of the heat-island effect of the city of Valencia, Spain through air temperature transets and NOAA satellite data. *Theoretical and Applied Climatology*, *43*, 195–203.

Dandou, A., Tombrou, M., & Soulakellis, N. (2009). The influence of the city of Athens on the evolution of the sea-breeze front. *Boundary-Layer Meteorology*, *131*, 35–51.

Dousset, B., & Gourmelon, F. (2003). Satellite multi-sensor data analysis of urban surface temperatures and land cover. *ISPRS Journal of Photogrammetry and Remote Sensing*, *58*, 43–54.

Founda, D., & Giannakopoulos, C. (2009). The exceptionally hot summer of 2007 in Athens, Greece—A typical summer in the future climate? *Global and Planetary Change*, *67*, 227–236.

Gallo, K. P., McNab, A. L., Karl, T. R., Brown, J. F., Hood, J. J., & Tarpley, J. D. (1993). The use of a vegetation index for assessment of the Urban Heat Island effect. *International Journal of Remote Sensing*, *14*, 2223–2230.

Gallo, K. P., McNab, A. L., Karl, T. R., Brown, J. F., Hood, J. J., & Tarpley, J. D. (1993). The use of NOAA AVHRR data for assessment of the Urban Heat Island effect. *Journal of Applied Meteorology*, *32*, 899–908.

Gallo, K. P., & Owen, T. W. (1998). Assessment of Urban Heat Island: A multisensor perspective for the Dallas-Ft. Worth, USA region. *Geocarto International*, *13*, 35–41.

Hung, T., Uchihama, D., Ochi, S., & Yasuoka, Y. (2006). Assessment with satellite data of the Urban Heat Island effects in Asian mega cities. *International Journal of Applied Earth Observation and Geoinformation*, *8*, 34–48.

Imhoff, M. L., Zhang, P., Wolfe, R. E., & Bounoua, L. (2010). Remote sensing of the Urban Heat Island effect across biomes in the continental USA. *Remote Sensing of Environment*, *114*, 504–513.

Jiménez-Muñoz, J. C., & Sobrino, J. A. (2008). Split-window coefficients for land surface temperature retrieval from low-resolution thermal infrared sensors. *IEEE Geoscience and Remote Sensing Letters*, *5*, 806–809.

Kidder, S. Q., & Wu, H. T. (1987). A multispectral study of the St. Louis area under snow-covered conditions using NOAA-7 AVHRR data. *Remote Sensing of Environment*, *22*, 159–172.

Kim, H. H. (1992). Urban Heat Island. *International Journal of Remote Sensing*, *13*, 2319–2336.

Lagouarde, J. -P., & Irvine, M. (2008). Directional anisotropy in thermal infrared measurements over Toulouse city center during the CAPITOUL measurement campaigns: First results. *Meteorol Atmos Phys.*, *102*, 173–185.

Lee, H. -Y. (1993). An application of NOAA AVHRR thermal data to the study of Urban Heat Islands. *Atmospheric Environment*, *27B*, 1–13.

Livada, I., Santamouris, M., Niachou, K., Papanikolaou, N., & Mihalakakou, G. (2002). Determination of places in the great Athens area where the heat island effect is observed. *Theoretical and Applied Climatology*, *71*, 219–230.

Lo, C. P., Quattrochi, D. A., & Luvall, J. C. (1997). Application of high resolution thermal infrared remote sensing and GIS to assess the Urban Heat Island effect. *International Journal of Remote Sensing*, *18*, 287–304.

Nichol, J. E. (1994). A GIS based approach to microclimate monitoring in Singapore's high rise housing estates. *Photogrammetric Engineering and Remote Sensing*, *60*, 1225–1232.

Nichol, J. E. (1996). Analysis of the urban thermal environment with LANDSAT data. *Environment and Planning B: Planning and Design*, *23*, 733–747.

Nichol, J. E. (1998). Visualization of urban surface temperatures derived from satellite images. *International Journal of Remote Sensing*, *19*, 1639–1649.

Nichol, J., & Wong, W. S. (2005). Modeling urban environmental quality in a tropical city. *Landscape and Urban Planning*, *73*, 49–58.

Oke, T. R. (1982). The energetic basis of the Urban Heat Island. *Quarterly Journal of the Royal Meteorological Society*, *108*, 1–24.

Oke, T. R. (1987). *Boundary layer climates.* Cambridge: University Press.

Owen, T. W., Carlson, T. N., & Gillies, R. R. (1998). An assessment of satellite remotely sensed land cover parameters in quantitatively describing the climatic effect of urbanization. *International Journal of Remote Sensing*, *19*, 1663–1681.

Pal, N. R., & Pal, S. K. (1993). A review on image segmentation techniques. *Pattern Recognition*, *26*, 1277–1294.

Pu, R., Gong, P., Michishita, R., & Sasagawa, T. (2006). Assessment of multi-resolution and multi-sensor data for urban surface temperature retrieval. *Remote Sensing of Environment: Thermal Remote Sensing of Urban Areas*, *104*, 211–225.

Rajasekar, U., & Weng, Q. (2009). Urban Heat Island monitoring and analysis by data mining of MODIS imageries. *ISPRS Journal of Photogrammetry and Remote Sensing*, *64*, 86–96.

Roth, M., Oke, T. R., & Emery, W. J. (1989). Satellite-derived Urban Heat Island from three coastal cities and the utilization of such data in urban climatology. *International Journal of Remote Sensing*, *10*, 1699–1720.

Santamouris, M., Paraponiaris, K., & Mihalakakou, G. (2007). Estimating the ecological footprint of the heat island effect over Athens, Greece. *Climatic Change*, *80*, 265–276.

Sobrino, J. A., Jiménez-Muñoz, J. C., Sòria, G., Romaguera, M., Guanter, L., Moreno, J., et al. (2008). Land surface emissivity retrieval from different VNIR and TIR sensors. *IEEE Transactions on Geoscience and Remote Sensing*, *46*, 316–327.

Sobrino, J. A., Kharraz, E. J., & Li, Z. -L. (2003). Surface temperature and water vapour retrieval from MODIS data. *International Journal of Remote Sensing*, *20*, 5161–5182.

Sobrino, J. A., Raissouni, N., & Li, Z. -L. (2001). A comparative study of land surface emissivity retrieval from NOAA data. *Remote Sensing of Environment*, *75*, 256–266.

Sobrino, J. A., Raissouni, N., Simarro, J., Nerry, F., & Petitcolin, F. (1999). Atmospheric water vapor content over land surfaces derived from the AVHRR data: Application to the Iberian Peninsula. *IEEE Transactions and Geoscience and Remote Sensing*, *37*, 1425–1434.

Stathopoulou, M., & Cartalis, C. (2007). Daytime Urban Heat Islands from Landsat ETM + and Corine land cover data: An application to major cities in Greece. *Solar Energy*, *81*, 358–368.

Stathopoulou, M., & Cartalis, C. (2007). Use of satellite remote sensing in support of Urban Heat Island studies. *Advances in Building Energy Research*, *1*, 203–212.

Stathopoulou, M., & Cartalis, C. (2009). Downscaling AVHRR land surface temperatures for improved surface Urban Heat Island intensity estimation. *Remote Sensing of Environment*, *113*, 2592–2605.

Stathopoulou, M., Cartalis, C., & Keramitsoglou, I. (2004). Mapping micro-urban heat islands using NOAA/AVHRR images and CORINE Land Cover: an application to coastal cities of Greece. *International Journal of Remote Sensing*, *25*, 2301–2316.

Streutker, D. R. (2002). A remote sensing study of the Urban Heat Island of Houston, Texas. *International Journal of Remote Sensing*, *23*, 2595–2608.

Streutker, D. R. (2003). Satellite-measured growth of the Urban Heat Island of Houston, Texas. *Remote Sensing of Environment*, *85*, 282–289.

Voogt, J. A., & Oke, T. R. (2003). Thermal remote sensing of urban climate. *Remote Sensing of Environment*, *86*, 370–384.

Weng, Q. (2001). A remote sensing-GIS evaluation of urban expansion and its impact on surface temperature in the Zhujiang Delta, China. *International Journal of Remote Sensing*, *22*, 1999–2014.

Weng, Q. (2003). Fractal analysis of satellite-detected Urban Heat Island effect. *Photogrammetric Engineering and Remote Sensing*, *69*, 555–566.

Weng, Q. (2009). Thermal infrared remote sensing for urban climate and environmental studies: Methods, applications, and trends (Review article). *ISPRS Journal of Photogrammetry and Remote Sensing*, *64*, 335–344.

Weng, Q., Liu, H., Liang, B., & Lu, D. (2008). The spatial variations of urban land surface temperatures: pertinent factors, zoning effect, and seasonal variability. *IEEE Journal of Selected Topics in Applied Earth Observations & Remote Sensing*, *1*(2), 154–166.

Weng, Q., Lu, D., & Liang, B. (2006). Urban surface biophysical descriptors and land surface temperature variations. *Photogrammetric Engineering & Remote Sensing*, *72*, 1275–1286.

Weng, Q., Lu, D., & Schubring, J. (2004). Estimation of land surface temperature vegetation abundance relationship for Urban Heat Island studies. *Remote sensing of Environment*, *89*, 467–483.

Weng, Q., & Quattrochi, D. A. (2006). Thermal remote sensing of urban areas: An introduction to the special issue (Editorial). *Remote Sensing of Environment*, *104*, 119–122.

WIST web site Created by WIST, Version WIST-10.30.GA-1. https://wist.echo.nasa.gov/~wist/api/imswelcome/ (last accessed on 12/22/2010)

Xiao, R., Weng, Q., Ouyang, Z., Li, W., Schienke, E. W., & Zhang, W. (2008). Land surface temperature variation and major factors in Beijing, China. *Photogrammetric Engineering & Remote Sensing*, *74*, 451–461.